ChemElectroChem

Research Article
doi.org/10.1002/celc.202300286

Chemistry Europe
European Chemical Societies Publishing

www.chemelectrochem.org

Soluble Ruthenium Phthalocyanines as Semiconductors for Organic Thin-Film Transistors

José García-Calvo[+],[a, b, c] Rosemary R. Cranston[+],[d] Ismael López-Duarte,[e] Tomás Torres,*[a, b, c] and Benoît H. Lessard*[d, f]

Ruthenium phthalocyanine (RuPcs) are multipurpose compounds characterized by their remarkable reactivity and photoelectronic properties, which yield a broad synthetic scope and easy derivatization at the axial position. However, RuPcs have been underexplored for use in organic thin-film transistors (OTFTs), and therefore new studies are necessary to provide basic insight and a first approach in this new application. Herein, two novel RuPc derivatives, containing axial pyridine substituents with aliphatic chains (RuPc(CO)(PyrSiC6) (**1**) and $RuPc(PyrSiC6)_2$ (**2**), were synthesized, characterized, and tested as the organic semiconductor in OTFTs. RuPc thin-films were characterized by X-ray diffraction (XRD), and atomic force microscopy (AFM) to assess film morphology and microstructure. **1** displayed comparable p-type device performance to other phthalocyanine-based OTFTs of similar design, with an average field effect mobility of 2.08×10^{-3} $cm^2V^{-1}s^{-1}$ in air and 1.36×10^{-3} $cm^2V^{-1}s^{-1}$ in nitrogen, and threshold voltages from −11 V to −20 V. **2** was found to be non-functional as the semiconductor in the device architecture used, likely as a result of significant differences in thin-film formation. The results of this work illustrate a promising starting point for future development of RuPc electronic devices, particularly in this new family of OTFTs.

Introduction

Ruthenium phthalocyanines (RuPcs) have been studied for a wide array of applications, including materials chemistry,[1,2] photoelectronics,[3] and photodynamic therapy.[4–6] Additionally, RuPc compounds have found utility in a number of electronic devices, perhaps most prominently in organic photovoltaics (OPVs),[7–11] but have also been used in gas sensors,[12–15] and organic light emitting diodes (OLEDs).[16] However, to our knowledge, there are no reported accounts of RuPc compounds used as semiconductors in organic thin-film transistors (OTFTs). Using a three-electrode system to amplify or switch electrical signals, OTFTs are crucial for the development of complex organic electronic devices and typically consist of a semiconducting thin-film, an insulating dielectric layer, and the gate, source, and drain electrodes (Figure 1a).

The chemistry of RuPc derivatives is typically based on modifications to peripheral or axial positions. Due to the harsh conditions when forming the RuPc complexes,[17] variations in the periphery are restricted to simple groups like -H or -*t*Bu. However, the axial positions have multiple possible ligands, from carbonyl, to DMSO, thiols or pyridines; this fact is presented as a major advantage in comparison with other more synthetically restricted and less stable Pc derivatives. Similar to silicon phthalocyanines (R_2-SiPcs),[18–21] the relatively simple modification of the RuPc axial positions allows for greater tunability and specific compound tailoring for different material applications. Depending on the conditions of the synthesis and the starting materials, derivatives containing strong (RuPc(CO)) or labile ($RuPc(PhCN)_2$) substituents may be isolated. Labile ligands are an ideal starting point for derivatization since they may react in mild conditions with pyridines. Pyridine modified RuPc complexes retain the favourable photoelectrochemical

[a] *Dr. J. García-Calvo,[+] Prof. Dr. T. Torres*
Department of Organic Chemistry
Campus de Cantoblanco
Universidad Autónoma de Madrid
28049 Madrid, Spain
E-mail: tomas.torres@uam.es

[b] *Dr. J. García-Calvo,[+] Prof. Dr. T. Torres*
Institute for Advanced Research in Chemical Sciences (IAdChem)
Campus de Cantoblanco
Universidad Autónoma de Madrid
28049 Madrid, Spain

[c] *Dr. J. García-Calvo,[+] Prof. Dr. T. Torres*
IMDEA-Nanociencia
Campus de Cantoblanco, c/Faraday 9
28049 Madrid, Spain

[d] *R. R. Cranston,[+] Prof. Dr. B. H. Lessard*
Department of Chemical and Biological Engineering
University of Ottawa
161 Louis Pasteur, Ottawa, Canada
Website: www.benoitlessard.ca
E-mail: benoit.lessard@uottawa.ca

[e] *Dr. I. López-Duarte*
Department of Chemistry in Pharmaceutical Sciences
Ciudad Universitaria
Complutense University of Madrid
Ramón y Cajal Square, 28040 Madrid, Spain

[f] *Prof. Dr. B. H. Lessard*
School of Electrical Engineering and Computer Science
University of Ottawa
800 King Edward Ave, Ottawa, Canada

[+] *These authors contributed equally to this work.*

Supporting information for this article is available on the WWW under https://doi.org/10.1002/celc.202300286

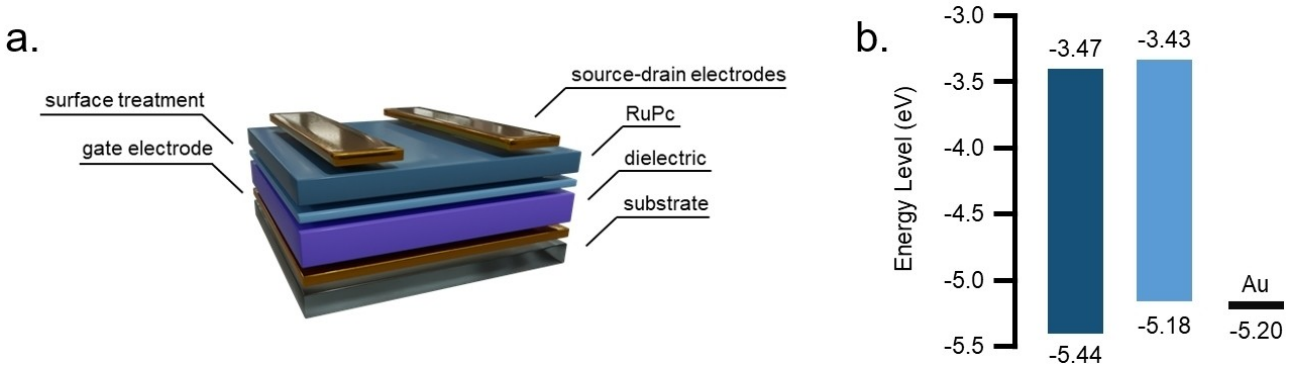

Figure 1. (a) Schematic diagram of bottom-gate top-contact OTFT architecture used in this work. (b) Differential of the energy levels calculated from the corresponding HOMO-LUMO gap of **1** (dark blue) and **2** (light blue).

properties but can alter solubility, photo- and thermo-stability or provide additional features related to the specific substituents used.[4,8,15,16] RuPcs typically lead to devices with p-type charge transport characteristics, which have been shown to increase in conductivity upon exposure to air, leading to improved performance.[9] For p-type OTFT operation, a negative voltage is applied to the gate which induces positive charges at the source electrode. The Fermi level of the electrode should closely match the HOMO level of the RuPc complex, such that a conducting channel forms at the dielectric-semiconductor interface. Applying a second voltage to the drain results in charge transport from the source to drain electrode indicative of p-type semiconducting materials.[22] We hypothesize that the introduction of alkylated substituents provides particularly high solubility in organic solvents, inducing favourable solid state microstructures when deposited, similar to what has been previously observed in other phthalocyanine derivatives.[23]

Herein we report the synthesis and characterization of two novel RuPc complexes RuPc(CO)(PyrSiC6) (**1**) and RuPc(PyrSiC6)$_2$ (**2**). The optical and electrochemical properties of each compound were measured and the HOMO and LUMO energy levels estimated (Figure 1b). RuPc complexes were used as the semiconductor in solution fabricated bottom-gate top-contact OTFTs, and characterized in air and nitrogen environments. Thin-film x-ray diffraction (XRD) and atomic force microscopy (AFM) were used to assess the film microstructure and morphology of each compound. This work show cases the utility of novel soluble RuPc complexes as semiconductors in a device application, emphasizing their favourable device performance in air.

Experimental Section

Materials

Chemical reagents were purchased from different sources, $Ru_3(CO)_{12}$ (98%) was provided by BLD pharmaceuticals, phthalonitrile (99%) was provided by TCI Chemicals, chlorotrihexylsilane (95%) and 4-pyridinemethanol (99%) were provided by Merck and solvents were purchased from Merck-Sigma Aldrich or Scharlab, and used as received unless otherwise specified. Hexamethyldisilane (HMDS, 98+%) was obtained from Thermo Fischer Scientific and anhydrous toluene (99.8%) was obtained from Merck-Sigma-Aldrich.

RuPc Synthesis

1. In a 10 mL flask RuPcCO **3** (50 mg, 78 μmol) was dissolved in tetrahydrofuran (THF, 3 mL) under argon atmosphere, compound **5** (61 mg, 156 μmol) was added to the solution and subsequently heated at reflux for 3 hrs. The mixture was concentrated under vacuum and purified by size exclusion chromatography on BioBeads SX-3 using an eluent of chloroform ($CHCl_3$), affording compound **1** as a dark blue solid powder.

Yield: 25 mg (31%). ^{1}H NMR ($CDCl_3$, 500 MHz): 9.39 (dd, $J^3_{H-H}=5.6$, $J^4_{H-H}=3.0$ Hz, 8H, CH), 8.09 (dd, $J^3_{H-H}=5.6$, $J^4_{H-H}=3.0$ Hz, 8H, CH), 5.28 (d, $J^3_{H-H}=7.0$ Hz, 2H, CH), 3.49 (s, 2H, CH_2), 1.94 (d, $J^3_{H-H}=7.0$ Hz, 2H, CH), 1.08–1.01 (m, 6H, CH_2), 0.98–0.92 (m, 12H, CH_2), 0.81 (d, $J=8.6$ Hz, 6H, CH_2), 0.71 (t, $J^3_{H-H}=7.3$ Hz, 9H, CH_3), 0.13–0.07 (m, 6H, CH_2). ^{13}C NMR ($CDCl_3$, 126 MHz): 178.7 (C), 151.1 (C), 144.3 (C), 143.8 (CH), 140.0 (C), 129.0 (CH), 122.2 (CH), 119.8 (CH), 61.3 (CH_2), 33.0 (CH_2), 31.3 (CH_2), 22.7 (CH_2), 22.5 (CH_2), 14.1 (CH_3), 13.0 (CH_2). IR (neat): 2885 (s), 2845 (s), 2771 (s), 1822 (s), 1584 (w), 1303 (w), 1270 (m), 1223 (m), 1132 (s), 1086 (m), 958 (w), 911 (w), 896 (w), 847 (w). HRMS (ESI$^+$) *m/z* calcd for $C_{57}H_{61}N_9O_2RuSi$ ($M+H^+$): 1034.3849; found: 1034.3827. UV-Vis (λ_{643}, $CHCl_3$) = 77591 M^{-1} cm^{-1}.

2. In a 10 mL flask, RuPc(NCPh)$_2$ **2** (100 mg, 0.12 mmol) was dissolved in $CHCl_3$ (8 mL) under argon atmosphere. Compound **5** (144 mg, 0.37 mmol) was added to the solution and stirred at room temperature for 18 hrs. The solution was directly purified by size exclusion chromatography on BioBeads SX-3 using an eluent of $CHCl_3$, affording compound **2** as a dark blue waxy solid.

Yield: 81 mg (49%). ^{1}H NMR ($CDCl_3$,500 MHz): 9.34–9.01 (m, 8H, CH), 7.88 (m, 8H, CH), 5.20 (d, $J=6.2$ Hz, 4H, CH), 3.48 (s, 4H, CH_2), 2.62–2.29 (m, 4H, CH), 1.13–0.84 (m, 48H, CH_2), 0.72 (t, $J=7.0$ Hz, 18H, CH_3), 0.24–0.01 (m, 12H, CH_2). ^{13}C NMR ($CDCl_3$, 125 MHz): 149.4 (CH), 148.5 (C), 143.8 (C), 141.0 (C), 128.0 (CH), 121.4 (CH), 119.5 (CH_2), 61.4 (CH_2), 33.0 (CH_2), 31.3 (CH_2), 22.7 (CH_2), 22.5 (CH_2), 14.1 (CH_3), 13.1 (CH_2). IR: 2876 (s), 2843 (s), 2771 (s), 1305 (s), 1270 (m), 1226 (m), 1186 (w), 1128(m), 1090 (m), 961 (s), 913 (s), 882 (m), 852 (m), 787 (w). HRMS (MALDI$^+$, DCTB) *m/z* calcd for $C_{80}H_{106}N_{10}O_2RuSi_2$ ($M+H^+$): 1397.7176; found: 1397.7131. UV-Vis (λ_{625} $CHCl_3$) = 43543 $M^{-1}cm^{-1}$.

RuPc Characterization

NMR were performed on a Bruker 300 MHz or 500 MHz at room temperature. ^{1}H NMR and ^{13}C·NMR were recorded on Bruker XRD-300 (300 MHz) and/or Bruker XRD-500 (500 MHz) instruments at room temperature (25 °C) and are reported as chemical shifts (δ) in ppm relative to TMS (δ = 0). Spin multiplicities are reported as a singlet (s), doublet (d), triplet (t) and quartet (q) with coupling constants (*J*) given in Hz, or multiplet (m). Mass spectrometry (MS) and high-resolution mass spectrometry (HRMS) spectra were recorded employing electrospray ionization (ESI Positive TOF_MS) mass spectra using a MAXIS II spectrometer, or matrix assisted laser desorption/ionization-time of flight (MALDI-TOF) using a Bruker Ultraflex III TOF/TOF spectrometer. IR spectra were recorded on an Agilent Technology Cary 630 FT-IR spectrometer (ATR) and are reported as wavenumbers υ in cm^{-1} with band intensities indicated as s (strong), m (medium), w (weak), br (broad). Molecular absorption spectroscopy (UV-vis) spectra were recorded on a JASCO–V660 spectrophotometer with a Jasco Peltier ETCS-761 temperature controller, using 10×10 mm quartz cuvettes and $CHCl_3$ as the solvent. Cyclic voltammetry (CV) measurements were carried out using a potentiostat/galvanostat instrument from Metrohm Autolab with a Glass Carbon work electrode (1 mm) under argon, an Ag/Ag^{+} reference electrode, and a platinum counter electrode. Ferrocene voltammograms were recorded as reference standards. Different potentials were applied to **1** and **2** (5×10^{-4} M) dissolved in THF with $(n\text{-}Bu)_4NPF_6$ (0.1 M) as the supporting electrolyte. The electrochemical waves are represented against Ferrocenium/Ferrocene redox process. The sweep rate was 100 mV s^{-1} and solutions were degassed with argon for 30 s before measurements. The value of the band gap was calculated from the first reduction/oxidation potentials obtained in the differential voltammetry and the energy levels from the following equation:[24]

$$E_{HOMO/LUMO} = -(E_{[onset,ox/red\ vs.\ Fc+/Fc]} + 5.1)\ (eV) \quad (1)$$

OTFT Fabrication and Characterization

Bottom-gate top-contact RuPc OTFTs were fabricated on 15 mm×20 mm silicon substrates with a 300 nm thick thermally grown silicon oxide dielectric layer purchased from Ossilla. To clean the substrate surface and to remove the protective photoresist, sequential sonication baths of soapy water, de-ionized water, acetone, and methanol were used. The substrates were then dried with nitrogen and treated with air plasma for 10 min before applying the surface treatment. Surface treatment of HMDS was carried out in a nitrogen environment by spin coating 50 µl of HMDS onto substrates at 3000 RPM for 30 sec, then drying at 150 °C for 1 hr under vacuum. Solutions of **1** and **2** at a concentration of 10 mg ml^{-1} in toluene were prepared by heating at 50 °C for 1 hr, then filtering through 0.45 µm pore size PTFE membranes. Thin-films were fabricated by depositing the RuPc solutions onto HMDS treated substrates by spin-coating 50 µl of solution at 3000 RPM for 30 sec. The thin-films were then dried under vacuum at 70 °C for 1 hr to remove any residual solvent. Top-contact, 50 nm thick, gold electrodes were deposited by physical vapour deposition using an Angstrom EvoVac thermal evaporator ($P < 2\times10^{-6}$ torr) at a rate of 1 Å s^{-1}.

Electrical characterization of OTFTs was done in air and nitrogen environments at room temperature using a multi tester consisting of 48 gold plated nickel probe tips that contact the source-drain and gate electrodes of each transistor on the substrate simultaneously. A Keithley 2614B and a MCC USB DAQ was used to control the source-drain voltage ($V_{SD} = -50$ V) and gate voltage ($0\ V < V_{GS} < -60$ V) to obtain source-drain current (I_{SD}) measurements. The average hole field effect mobility (μ_h), average threshold voltage (V_T), and on/off current ratio ($I_{on/off}$) was calculated by the MOSFET model.[25]

Thin-film Characterization

AFM images were taken using a Bruker Dimension Icon AFM with ScanAsyst-Air tips at a rate of 0.814 Hz and analyzed using NanoScope Analysis v.1.8 software. XRD measurements were obtained using a Rigaku Ultima IV powder diffractometer with a Cu Kα ($\lambda = 1.5418$ Å) source, a scan range of $4 < 2\theta < 15°$, and rate of 0.5° min^{-1}. The *d*-spacing between successive parallel diffraction planes was calculated using Bragg's Law.

Results and Discussion

Synthesis of RuPc Complexes

Herein the synthesis and characterization of two novel RuPc complexes are reported, with Figure 2 illustrating the synthetic pathway used to produce compound **1** and **2** displayed in Figure 1a. The starting materials for the RuPc complexes, RuPcCO and $RuPc(PhCN)_2$, were prepared following procedures adapted from literature.[17] $Ru_3(CO)_{12}$ was condensed with neat phthalonitrile, by heating at reflux in o-dichlorobenzene or benzonitrile, to obtain RuPcCO (**3**) or $RuPc(PhCN)_2$ (**4**), respectively. The pyridine derivative **5** was synthesized according to reported procedures.[4] Chlorotrihexylsilane was combined with pyridin-4-ylmethanol at room temperature to obtain pyridine **5**, with ^{1}H NMR and ^{13}C NMR reported in **Figure S1** and **Figure S2**. Final RuPc complexes were obtained by following standardized methods for these types of pyridine complexes. RuPc(CO)(PyrSiC6) (**1**) was obtained by coordinating RuPc(CO) (**3**) to the corresponding pyridine **5** in THF, heating under reflux for 3 hrs and isolating the product by size exclusion chromatography. ^{1}H NMR, ^{13}C NMR, and HRMS of **1** are reported in **Figure S3**, **Figure S4**, and **Figure S5**. Similarly, $RuPc(PyrSiC6)_2$ (**2**) was obtained from $RuPc(PhCN)_2$ (**4**) plus the corresponding pyridine **5** in $CHCl_3$, by stirring at room temperature for 18 hrs and following the same purification process by size exclusion chromatography. ^{1}H NMR, ^{13}C NMR, and HRMS of **2** are reported in **Figure S6**, **Figure S7**, and **Figure S8**. Once concentrated under vacuum **1** (yield of 31%) and **2** (yield of 49%) were obtained as a blue solid powder and as a waxy solid, respectively.

UV-Vis Absorption and Electrochemical Properties

The optical and electrochemical properties of RuPc complexes **1** and **2** were measured in $CHCl_3$ solutions with results displayed in Figure 3a. For both **1** and **2**, no fluorescence in the UV-vis region was observed, with the characteristic intense Soret band maximized at 298 nm and 315 nm, respectively. The di-substituted complex **2** exhibits a more intense Soret band which is in agreement for the general results of these

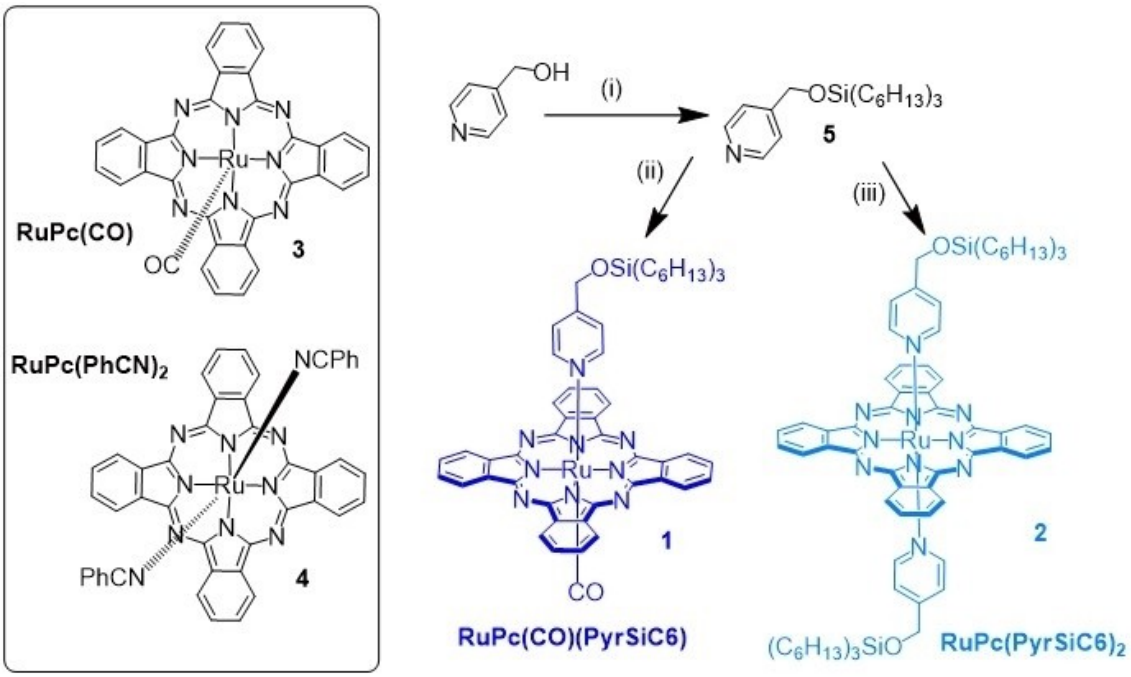

Figure 2. Synthetic pathway to produce RuPc complexes used in this work. (i) Chlorotrihexylsilane, imidazole, DMF/CH_2Cl_2 (9:1), 16 hrs, 89%; (ii) THF, reflux, 3 hrs, 31%; (iii) $CHCl_3$, reflux, 18 hrs, 49%.

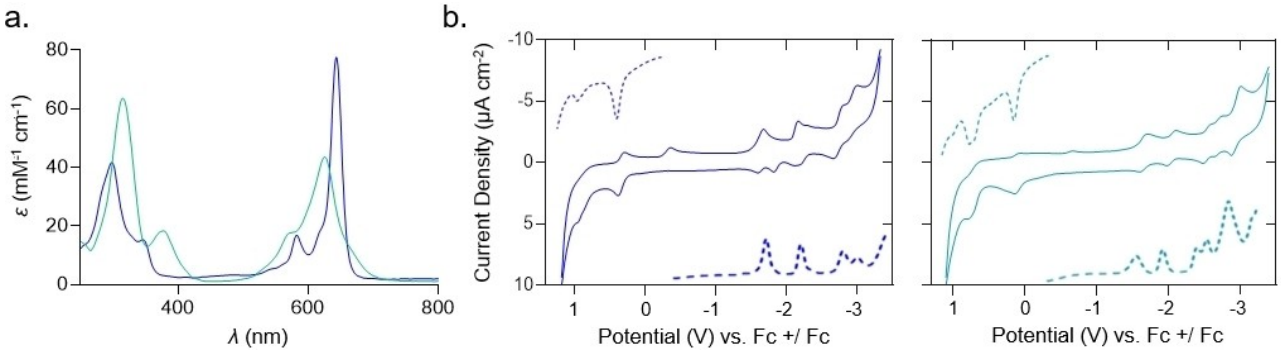

Figure 3. (a) UV-vis spectra of **1** (dark blue) and **2** (light blue) in $CHCl_3$. (b) Cyclic and differential-pulse voltammograms of **1** (dark blue) and **2** (light blue) in THF; relative differential pulse voltammetry is indicated by dashed lines.

complexes.[7] The Q-band maximum for compound **1** is obtained at 643 nm, while for compound **2**, it is at 625 nm with a shoulder. In comparison to compound **2**, the Q-band of **1** is sharper and exhibits a higher molar extinction coefficient (λ_{643} = 77600 $M^{-1}cm^{-1}$ for **1**, λ_{625} = 43500 $M^{-1}cm^{-1}$ for **2**); associated with a lower tendency for aggregation and a more defined separation between energy levels. Additionally, the absorbance ratio was checked at different concentrations, with a linear behaviour from 1 to 15 μM. Diffusion controlled CV studies were performed for compounds **1** and **2**, which were dissolved in THF to assess the impact of the mono/di-substituted complex over the redox potentials, as presented in Figure 3b. The experiments are delivered against the redox potential of ferrocenium/ferrocene, noticing a similar redox curve shape for both compounds. Between 0.5 to −2.5 V one reversible oxidation potential and two reductions happened. The calculated experimental electrochemical band gap of the carbonyl compound **1** was wider in comparison with compound **2**, 1.97 eV against 1.75 eV, respectively (Figure 1c). These results already suggested a prospective better electrical performance of compound **1** in devices.

Organic Thin-Film Transistors

OTFTs were fabricated using **1** and **2** as the semiconducting layer and characterized at room temperature in nitrogen and air environments to assess the electrical performance by determining μ_h, V_T, and $I_{on/off}$. Compound **2** was found to be non-functional in OTFTs, while compound **1** displayed p-type charge transport in both air and nitrogen resulting in operating devices. Additionally, **Figure S9** displays a comparison between

the p-type and n-type semiconducting properties of **1** when operated in nitrogen, with **1** exhibiting no electron charge transport. Figure 4a depicts the characteristic p-type forward and reverse transfer curves of **1** in both testing environments, with a characteristic output curve of **1** in air displayed in **Figure S10**. The spin speed and time used for deposition was varied (**Figure S11**, **Table S1**, and **Figure S12**) to determine principal fabrication conditions of 3000 RPM and 30 sec.

In air, **1** exhibited an average μ_h of $2.08\pm0.81\times10^{-3}\,cm^2V^{-1}s^{-1}$ with a maximum μ_h of $7.85\times10^{-3}\,cm^2V^{-1}s^{-1}$, an average V_T of -11.2 ± 1.4 V and an $I_{on/off}$ of 10^3. While in nitrogen, OTFTs using **1** as the semiconducting layer yielded a lower average and maximum μ_h of $1.36\pm2.00\times10^{-3}\,cm^2V^{-1}s^{-1}$ and $3.72\times10^{-3}\,cm^2V^{-1}s^{-1}$ respectively, a lower average V_T of -19.7 ± 1.8 V with the same $I_{on/off}$ of 10^3. Higher μ_h and improved V_T with operation in air is expected of p-type OTFTs as exposure to oxygen has been shown to increase the work function and improve the conductivity of p-type MPc thin-films.[26–29] P-doping in air is thought to be a result of a higher concentration of mobile holes due to adsorbed oxygen,[27] and the preferential interaction between oxygen and gap states at grain boundaries which improves device performance by decreasing charge trapping and recombination.[29] Additionally, the increased conductivity in RuPc thin-films when exposed to air has been known to improve the performance of photovoltaic devices.[9] The electrical performance of **1** OTFTs is consistent with other p-type MPc OTFTs fabricated by both solution and solid state processes which typically display μ_h from $1–10^{-3}\,cm^2V^{-1}s^{-1}$ with V_T ranging from 5 V to −20 V, and $I_{on/off}$ between $10^3–10^5$.[23,30]

The difference in device performance between compounds **1** and **2** can be attributed to several factors, such as the redox potentials, but it is likely to be mainly because of the variations in thin-film microstructure and morphology; factors that heavily influence OTFT performance of MPcs.[31–33] Figure 4b displays the XRD pattern of **1** and **2** thin-films, with both materials exhibiting a low angle diffraction peak at $2\theta=4.14°$ (*d*-spacing of 21.3 Å) and 4.36° (*d*-spacing of 20.2 Å) respectively. In addition, compound **1** displays a slightly higher intensity diffraction peak at $2\theta=5.30°$ corresponding to a intermolecular *d*-spacing of 16.7 Å. The second diffraction peak of compound **1** indicates a population of molecules arranged in a more ordered and densely packed microstructure. We surmise this microstructure enables effective charge transport between molecules, compared to compound **2** where that the intermolecular spacing is too large and is partially the reason for non-functional OTFTs. AFM images (Figure 4c and Figure 4d) reveal considerable differences in surface morphology between **1** and

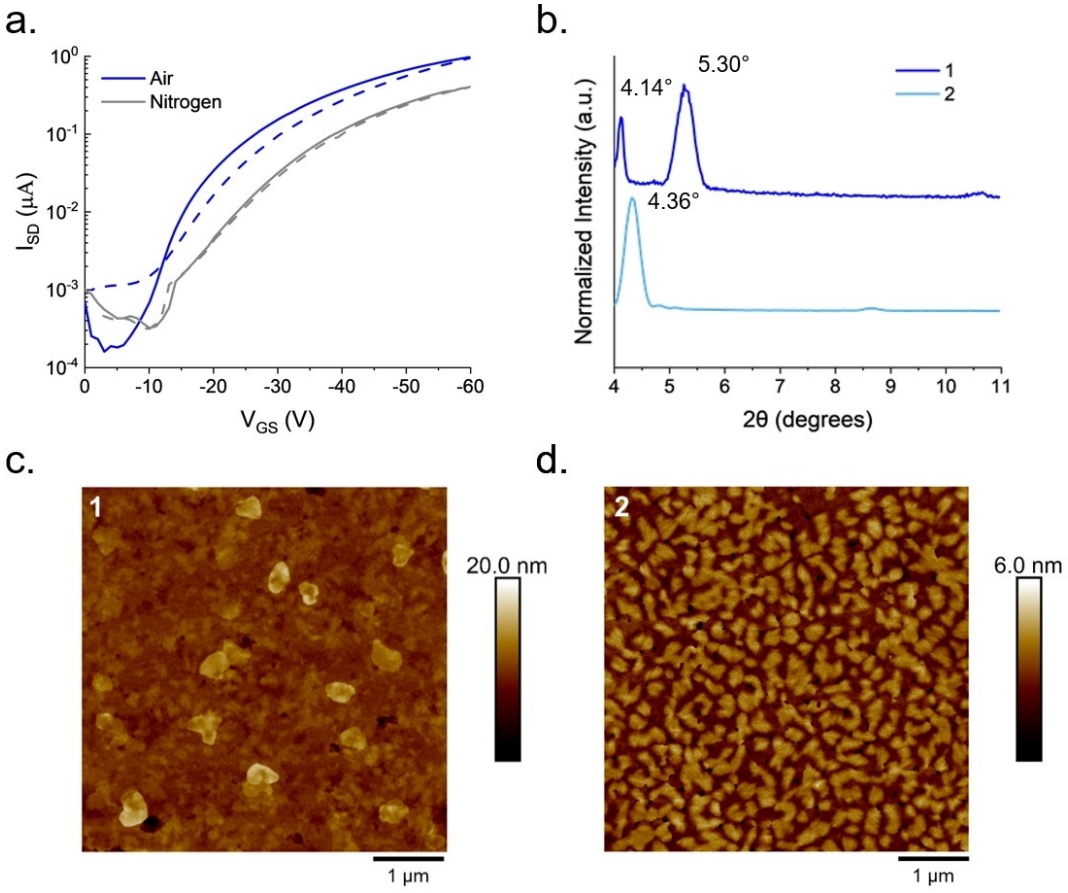

Figure 4. (a) Characteristic transfer curves of OTFTs using **1** as the semiconductor characterized at room temperature in nitrogen and air, with solid and dashed lines representing the forward and reverse sweeps respectively. (b) XRD patterns of **1** and **2** thin-films. AFM images (5 μm×5 μm) of (c) **1** and (d) **2** with a scale bar of 1.0 μm.

2. Compound **1** exhibits large platelet features with limited grain boundaries, and a surface roughness of 1.26 nm, whereas thin films of compound **2** result in a sparse network of crystallites with large grain boundaries, and a surface roughness of 0.752 nm. Although **2** has a lower surface roughness, the large gaps between grains likely hinder charge transport and contributes to the lack of semiconducting behaviour in devices.

Conclusions

Herein, the synthesis of a novel family of RuPc derivatives is presented, and successfully applied to the development of OTFTs. The use of alkyl-substituted pyridine gave favourable results in the case of the single substituted carbonyl RuPc derivative, RuPc(CO)(PyrSiC6) (**1**), with device performance comparable to other p-type phthalocyanine based OTFTs. Spin speed and time during thin-film deposition were varied to determine the optimal fabrication conditions for this derivative, which exhibited an average field effect mobility of 2.08×10^{-3} $cm^2V^{-1}s^{-1}$ in air and 1.36×10^{-3} $cm^2V^{-1}s^{-1}$ in nitrogen, and threshold voltages ranging from −11 V to −20 V dependant on the operating environment. The double substituted RuPc, $RuPc(PyrSiC6)_2$ (**2**), yielded non-functional devices as a result of a less ideal thin-film microstructure and surface morphology as indicated by the large *d*-spacing and uneven sparse crystallite network observed in films. Overall, this work represents a first step in the application of solution processable RuPcs, that may be easily modified with different ligands and tested as a semiconductor layer for OTFTs; highlighting an emerging opportunity for new variations in an underexplored family of phthalocyanines.

Supporting Information

The Supporting Information is available free of charge.

^{1}H NMR and ^{13}C NMR spectra of compounds **1**, **2**, and **5** in $CDCl_3$. HRMS (ESI^+) of compound **1** and **2**. Characteristic output curve of compound **1** in air. Transfer curves, XRD patterns, AFM images, and a summary of the transistor characteristics of OTFTs using compound **1**, deposited at different spin speeds. Transfer curves, XRD patterns, and a summary of the transistor characteristics of OTFTs using compound **1**, deposited at different spin times.

Funding Sources

J.G.C. acknowledges his funding from "Ayudas María Zambrano para la atracción de talento internacional" and "Ayudas de atracción de talento de la Comunidad de Madrid 2022". T.T. acknowledges financial support from the Spanish AEI/MICINN (PID2020-116490GB-I00, TED2021-131255B-C43) and the Comunidad de Madrid and the Spanish State through the Recovery, Transformation and Resilience Plan ["Materiales Disruptivos Bidimensionales (2D)" (MAD2D-CM) (UAM1)-MRR Materiales Avanzados], and the European Union through the Next Generation EU funds. IMDEA Nanociencia acknowledges support from the "Severo Ochoa" Programme for Centres of Excellence in R&D (MINECO, Grant SEV2016-0686).

The Natural Sciences and Engineering Research Council of Canada (NSERC, RGPIN/2015-509 03987 and STPGP 506661-17 to B.H.L.) and the University of Ottawa are acknowledged for financial support. The research was undertaken thanks to funding from the Canada Research Chair Program in which B.H.L. is a member.

Author Contributions

R.R.C. and J.G.C. are co-first authors. The manuscript was written through the contributions of all authors. All authors have given approval to the final version of the manuscript. R.R.C. and J.G.C conducted the experimental work, data analysis, and wrote the initial draft of the manuscript. J.G.C. performed the synthesis and characterization of the RuPc complexes, and UV-vis/CV experiments. R.R.C fabricated and characterized OTFTs and performed AFM, and XRD on RuPc thin-films. I.L.D. contributed with preliminary synthetic studies on RuPc. T.T and B.H.L. acquired funding, managed supervision, directed the study as well as assisted in editing the manuscript.

Acknowledgements

B.H.L and R.R.C would like to thank the Centre for Research in Photonics at the University of Ottawa (CRPuO) for access to the AFM.

Conflict of Interests

The authors declare no conflict of interest.

Data Availability Statement

The data that support the findings of this study are available in the supplementary material of this article.

Keywords: Organic Thin-Film Transistor · Photo-Electrochemical Characterization · p-Type Organic Semiconductor · Ruthenium Phthalocyanine · Solution Processing

[1] G. Mattioli, G. Contini, F. Ronci, R. Flammini, F. Frezza, R. Larciprete, V. Raglione, P. Alippi, F. Filippone, A. A. Bonapasta, G. Zanotti, B. Kierren, L. Moreau, T. Pierron, Y. Fagot-Revurat, S. Colonna, *J. Phys. Chem. C* **2023**, *127*, 3316.
[2] S. V. Zaitseva, E. Y. Tyulyaeva, D. V. Tyurin, S. A. Zdanovich, O. I. Koifman, *Polyhedron* **2022**, *217*, 115739.
[3] J. Joseph, L. M. O. Lourenço, J. P. C. Tomé, T. Torres, D. M. Guldi, *Nanoscale* **2022**, *14*, 13155.

[4] J. T. Ferreira, J. Pina, C. A. F. Ribeiro, R. Fernandes, J. P. C. Tomé, M. S. Rodríguez-Morgade, T. Torres, *Chem. A Eur. J.* **2020**, *26*, 1789.
[5] R. G. de Lima, R. R. Rios, A. E. da H. Machado, R. S. da Silva, *'Ruthenium phthalocyanines in nitric oxide modulation and singlet oxygen release: Selectivity and cytotoxic effect on cancer cell lines'*, **2022**, 355.
[6] G. Y. Atmaca, F. T. Elmalı, A. Erdoğmuş, *J. Mol. Struct.* **2023**, *1274*, 134332.
[7] M. K. R. Fischer, I. López-Duarte, M. M. Wienk, M. V. Martínez-Díaz, R. A. J. Janssen, P. Bäuerle, T. Torres, *J. Am. Chem. Soc.* **2009**, *131*, 8669.
[8] M. S. Rodríguez-Morgade, M. E. Plonska-Brzezinska, A. J. Athans, E. Carbonell, G. de Miguel, D. M. Guldi, L. Echegoyen, T. Torres, *J. Am. Chem. Soc.* **2009**, *131*, 10484.
[9] A. Capobianchi, M. Tucci, *Thin Solid Films* **2004**, *451–452*, 33.
[10] A. Morandeira, I. López-Duarte, B. O'Regan, M. V. Martínez-Díaz, A. Forneli, E. Palomares, T. Torres, J. R. Durrant, *J. Mater. Chem.* **2009**, *19*, 5016.
[11] R. Ehamparam, L. E. Oquendo, M. W. Liao, A. K. Brynnel, K.-L. Ou, N. R. Armstrong, D. V. McGrath, S. S. Saavedra, *ACS Appl. Mater. Interfaces* **2017**, *9*, 29213.
[12] A. M. Paoletti, G. Pennesi, G. Rossi, A. Generosi, B. Paci, V. R. Albertini, *Sensors* **2009**, *9*, 5277.
[13] G. Guillaud, J. Simon, J. P. Germain, *Coord. Chem. Rev.* **1998**, *178–180*, 1433.
[14] A. Generosi, V. R. Albertini, G. Rossi, G. Pennesi, R. Caminiti, *J. Phys. Chem. B* **2003**, *107*, 575.
[15] V. Rossi Albertini, A. Generosi, B. Paci, P. Perfetti, G. Rossi, A. Capobianchi, A. M. Paoletti, R. Caminiti, *Appl. Phys. Lett.* **2003**, *82*, 3868.
[16] Y. Zhu, C. Gu, S. Tang, T. Fei, X. Gu, H. Wang, Z. Wang, F. Wang, D. Lu, Y. Ma, *J. Mater. Chem.* **2009**, *19*, 3941.
[17] T. Rawling, A. McDonagh, *Coord. Chem. Rev.* **2007**, *251*, 1128.
[18] B. H. Lessard, *ACS Appl. Mater. Interfaces* **2021**, *13*, 31321.
[19] M. C. Vebber, T. M. Grant, J. L. Brusso, B. H. Lessard, *Langmuir* **2020**, *36*, 2612.
[20] B. King, O. A. Melville, N. A. Rice, S. Kashani, C. Tonnelé, H. Raboui, S. Swaraj, T. M. Grant, T. McAfee, T. P. Bender, H. Ade, F. Castet, L. Muccioli, B. H. Lessard, *ACS Appl. Electron. Mater.* **2021**, *3*, 325.
[21] M. C. Vebber, N. A. Rice, J. L. Brusso, B. H. Lessard, *ACS Appl. Energ. Mater.* **2022**, *5*, 3426.
[22] G. Horowitz, *J. Mater. Res.* **2004**, *19*, 1946.
[23] O. A. Melville, B. H. Lessard, T. P. Bender, *ACS Appl. Mater. Interfaces* **2015**, *7*, 13105.
[24] C. M. Cardona, W. Li, A. E. Kaifer, D. Stockdale, G. C. Bazan, *Adv. Mater.* **2011**, *23*, 2367.
[25] J. Zaumseil, H. Sirringhaus, *Chem. Rev.* **2007**, *107*, 1296.
[26] H. Yasunaga, K. Kojima, H. Yohda, K. Takeya, *J. Phys. Soc. Jpn.* **1974**, *37*, 1024.
[27] H. R. Kerp, K. T. Westerduin, A. T. van Veen, E. E. van Faassen, *J. Mater. Res.* **2001**, *16*, 503.
[28] O. A. Melville, T. M. Grant, B. Mirka, N. T. Boileau, J. Park, B. H. Lessard, *Adv. Electron. Mater.* **2019**, *5*, 1900087.
[29] P. K. Nayak, R. Rosenberg, L. Barnea-Nehoshtan, D. Cahen, *Org. Electron.* **2013**, *14*, 966.
[30] N. T. Boileau, R. Cranston, B. Mirka, O. A. Melville, B. H. Lessard, *RSC Adv.* **2019**, *9*, 21478.
[31] R. R. Cranston, M. C. Vebber, J. F. Berbigier, N. A. Rice, C. Tonnelé, Z. J. Comeau, N. T. Boileau, J. L. Brusso, A. J. Shuhendler, F. Castet, L. Muccioli, T. L. Kelly, B. H. Lessard, *ACS Appl. Mater. Interfaces* **2021**, *13*, 1008.
[32] R. R. Cranston, M. C. Vebber, N. A. Rice, C. Tonnelé, F. Castet, L. Muccioli, J. L. Brusso, B. H. Lessard, *ACS Appl. Electron. Mater.* **2021**, *3*, 1873.
[33] B. King, A. J. Daszczynski, N. A. Rice, A. J. Peltekoff, N. J. Yutronkie, B. H. Lessard, J. L. Brusso, *ACS Appl. Electron. Mater.* **2021**, *3*, 2212.

Manuscript received: June 21, 2023
Revised manuscript received: August 3, 2023
Version of record online: September 1, 2023